The application of novel segmentation software to create left atrial geometry for atrial fibrillation ablation: The implication of spatial resolution

Chye-Gen Chin[a,b,c], Fa-Po Chung[a,d], Yenn-Jiang Lin[a,d], Shih-Lin Chang[a,d], Li-Wei Lo[a,d], Yu-Feng Hu[a,d], Ta-Chuan Tuan[a,d], Tze-Fan Chao[a,d], Jo-Nan Liao[a,d], Chin-Yu Lin[a,d], Ting-Yung Chang[a,d], Cheng-I Wu[a,d], Chih-Min Liu[a,d], Jennifer Jeanne B. Vicera[a,e], Chun-Chao Chen[a,f], Chieh-Mao Chuang[a,g], Yi-Jen Chen[b,c], Ming-Hsiung Hsieh[b,c,*], Shih-Ann Chen[a,d]

[a]Department of Medicine, Division of Cardiology, Heart Rhythm Center, Taipei Veterans General Hospital, Taipei, Taiwan, ROC; [b]Department of Internal Medicine, Division of Cardiology, School of Medicine, College of Medicine, Taipei Medical University, Taipei, Taiwan, ROC; [c]Department of Internal Medicine, Division of Cardiovascular Medicine, Wan Fang Hospital, Taipei Medical University, Taipei, Taiwan, ROC; [d]Department of Medicine, National Yang-Ming University School of Medicine, Taipei, Taiwan, ROC; [e]University of Santo Tomas Hospital, Manila, Philippines; [f]Department of Internal Medicine, Division of Cardiology, Shuang Ho Hospital, Taipei Medical University, Taipei, Taiwan, ROC; [g]Division of Pediatric Cardiology, China Medical University Children's Hospital, China Medical University, Taichung, Taiwan, ROC

Abstract

Background: The application of new imaging software for the reconstruction of left atrium (LA) geometry during atrial fibrillation (AF) ablation has not been well investigated.

Methods: A total of 27 patients undergoing AF ablation using a CARTO Segmentation Module system were studied (phase I). High-density LA mapping using PentaRay was merged with computed tomography-based geometry from the auto-segmentation module. The spatial distortion between the two LA geometries was analyzed and compared using Registration Match View. The associated contact force on the two LA shells was prospectively validated in 16 AF patients (phase II).

Results: Of the five LA regions, the roof area had the highest quality score between the two LA shells (1.7 ± 0.6). In addition, among the pulmonary veins (PVs), higher quality scores were observed in bilateral PV carinas (both 1.8 ± 0.1, $p < 0.05$) than in the anterior or posterior PV regions. Furthermore, surrounding the PV ostium, the on-surface points had a significantly higher contact force when targeting the high-density fast anatomical mapping shell than for the auto-segmentation module (right superior pulmonary vein, 20.7 ± 5.8 g vs 12.5 ± 4.4 g; right inferior pulmonary vein, 19.3 ± 6.8 g vs 11.8 ± 4.8 g; left superior pulmonary vein, 22.5 ± 7.3 g vs 11.2 ± 4.5 g; left inferior pulmonary vein, 15.7 ± 6.9 g vs 9.7 ± 4.4 g, $p < 0.05$ for each group).

Conclusion: The CARTO Segmentation Module and Registration Match View provide better anatomic accuracy and less regional distortion of the LA geometry, and this can prevent excessive contact and potential procedural complications.

Keywords: Atrial fibrillation; CARTO Segmentation Mapping; Fast anatomical mapping; Left atrium geometry

1. INTRODUCTION

Pulmonary vein (PV) isolation is the cornerstone procedure of atrial fibrillation (AF) ablation, especially for individuals with paroxysmal AF.[1] The reconstruction of left atrium (LA) geometry three-dimensional (3D) geometry is important for effective and safe catheter ablation,[2] and the incorporation of LA geometry and electroanatomic mapping can help to achieve a wide area circumferential ablation with better outcomes[3] and reductions in radiation exposure[4] and procedural duration.[5] Clear visualization of the tissue interface is one of the keys to establish good catheter tip-tissue surface contact,[6,7] and successful ablation and prevention of complications remain critically dependent on appropriate catheter tip-tissue contact. Several methods have been proposed to create the LA anatomic shell, including point-by-point electroanatomic mapping, intracardiac echocardiography, and fast anatomical mapping (FAM). Of these, FAM allows for the rapid recreation of 3D chamber geometries by moving sensor-based catheters placed in the LA. Furthermore, a recent study demonstrated that the use of a multi-electrode catheter could facilitate the detection of residual PV gaps and improve ablation outcomes.[8] However, the creation of FAM using a multi-electrode catheter may overestimate the size of LA geometry and volume owing to distortion of the LA anatomy, which

*Author correspondence. Dr. Ming-Hsiung Hsieh, Division of Cardiology, Wan-Fang Hospital, Taipei Medical University, 111, Section 3, Hsin-Lung Road, Taipei 116, Taiwan, ROC. E-mail address: mhhsieh@tmu.edu.tw (M.-H. Hsieh)

Author contributions: Dr. Chye-Gen Chin and Dr. Fa-Po Chung contributed equally to this study.

Conflicts of interest: The authors declare that they have no conflicts of interest related to the subject matter or materials discussed in this article.

Journal of Chinese Medical Association. (2020) 83: 830-837.

Received December 16, 2019; accepted April 1, 2020.

doi: 10.1097/JCMA.0000000000000390.

<zdoi: 10.1097/JCMA.0000000000000390>

may then result in the delivery of ablation lesions away from the intended anatomical targets.[9,10] On the other hand, contact force ablation catheter-guided mapping has been reported to be better at preventing anatomical distortion than conventional FAM methods.[11] However, the anatomic distortion can only be attenuated in regions with adequate contact points. Moreover, the completion of adequate mapping points using a contact force ablation catheter is time-consuming.[12]

To address these issues, new imaging software, CARTO Segmentation Module (Biosense Webster, Diamond Bar, CA, USA), has recently been developed to improve the resolution of LA geometry. However, the accuracy and applicability of this technology have not been fully studied in clinical practice. Therefore, the aims of this study were to: (1) clarify anatomic differences between computed tomography (CT) geometry created by the CARTO Segmentation Module and CT geometry created manually; (2) investigate anatomical differences in LA geometry derived from PentaRay-created FAM and CARTO Segmentation module CT geometry; and (3) assess differences in contact force based on surface contours generated by integrated FAM and CT geometry derived from the CARTO Segmentation Module in patients with AF.

2. METHODS

2.1. Study design and population

2.1.1. Phase I study

This retrospective study enrolled 27 patients who underwent ablation for drug-refractory and symptomatic paroxysmal or persistent AF using the CARTO 3.0 mapping system version 4.3 (Biosense Webster, Diamond Bar, CA, USA) at Taipei Veterans General Hospital. The patients underwent 12-lead electrocardiography, 24-hour Holter monitoring, echocardiography, and CT angiography of the PVs prior to the procedure. 3D chamber geometry was created by manual CT segmentation and the CARTO Segmentation Module software (Biosense Webster, Diamond Bar, CA, USA). LA parameters including longitudinal diameter and transverse diameter, and PV parameters including cross-sectional area and the diameter were compared between the two geometry shells. All parameters were measured as previously described.[13,14]

We also evaluated regional discrepancies between the geometry shells derived from FAM using a 1-mm electrode spacing multi-electrode mapping catheter (PentaRay, Biosense Webster, Diamond Bar, CA, USA) and the CARTO Segmentation Module.

2.1.2 . Phase II study

In the phase II study, we prospectively enrolled 16 patients with symptomatic AF who underwent catheter ablation between August 2018 and November 2018. The image processing was performed in a manner similar to that in the phase I study. ThermoCool SmartTouch catheters (Biosense Webster) were used for ablation. To create ablation lesions on the FAM geometry, the ablation was guided by the FAM anatomic shells. We then graded the contact force of each ablation lesion on the area with a quality score of 1 or >1. This study was conducted at Taipei Veterans General Hospital in Taiwan and was approved by the Institutional Review Board of Taipei Veterans General Hospital (IRB: 2019-04-001CC) and the Department of Health, Taiwan. Written informed consent was obtained from all patients.

2.2. Cardiac computed tomography imaging

All patients underwent multi-detector computed tomography (MDCT) to reconstruct PV and LA anatomy. MDCT was performed on a Siemens Somatom Definition system with a 64-slice dual-source configuration (Siemens AG, Healthcare Sector, Erlangen, Germany) within 24 hours before the ablation procedure to avoid significant variations in LA anatomy and volume secondary to changes in preload and afterload conditions. Retrospective electrocardiogram-gated spiral scanning was performed with collimation of 1.2 mm during injection of 80 mL of contrast medium (Iomeron 400 mg I/mL, Bracco, Milan, Italy) at a flow rate of 4 mL/s. The cardiac telediastolic phase was automatically determined in patients with sinus rhythm, while manual determination was performed in patients with AF to minimize motion artifacts. The images were then acquired during the end-expiratory phase. Multi-planar reconstruction, maximum intensity projection, and volume rendering were used to define and describe the LA anatomy. LA volume was measured using dedicated volume analysis software (Syngo VE32B Volume, software version 1.0, 2008, Siemens AG). The LA was manually outlined on axial images using a 3-mm thickness sequence. MDCT images (slice thickness 1.5 mm, position increment 0.7 mm) were then stored on a CD and data were loaded into the image integration module of the mapping system (CARTOMERGER Module, Biosense Webster). Segmentation of the MDCT images was then performed as previously described,[5,15] and the LA contours were semi-automatically reconstructed and the volume was calculated. Ostial PV diameters, LA anterior–posterior, lateral-septal, and superior–inferior diameters were also manually measured. Isolated LA and PVs after 3D reconstruction were then exported to the mapping system for subsequent mapping and integration processes.

2.3. Cardiac computed tomography imaging and sub-segmentation of LA geometry

The CARTO Segmentation Module software was also used to create another LA geometry. The segmentation reconstruction was a combination of the two main methods: the first was intensity, using the scan data of 4,096 possible values, and the second was model-based. The combination of these two methods could yield the best segmentation results for both sides of the heart with high required accuracy. The workflow using the module has been described in a previous study.[16]

The LA body was divided into five sub-segments including roof, posterior wall, septum, anterior wall, and left lateral wall.[11] Fig. 1 illustrates an example of the LA sub-segments. The PVs were divided separately into three sub-segments per side, including anterior, posterior and carina.

2.4. Creation of Fast Anatomical Map (FAM)-based LA and PV Images

The creation of FAM-based LA and PV geometry has been described in previous studies.[17,18] A high-density mapping catheter (PentaRay, Biosense-Webster) was used in all cases for the generation of FAM. The average mapping sites in the left atria included more than 1800 points for each patient.

2.5. Comparison of FAM-based and CARTO Segmentation-derived 3D LA Geometries

The reconstructed CT data sets were merged with the geometries via three registration processes. Visual alignment was performed with the use of landmark pairs, that is, landmarks of the right PV carina, established on the FAM images, and corresponding sites on the reconstructed CT image.[19] After surface registration,[20,21] a manual iterative process was used to minimize differences in individual PV positions and overall LA geometry.[22] The spatial distortion between the two LA geometries was analyzed and compared to Registration Match View. The quality score was used to define the concordance of the two geometries, and quality scores of 1, 2, and 3 were defined

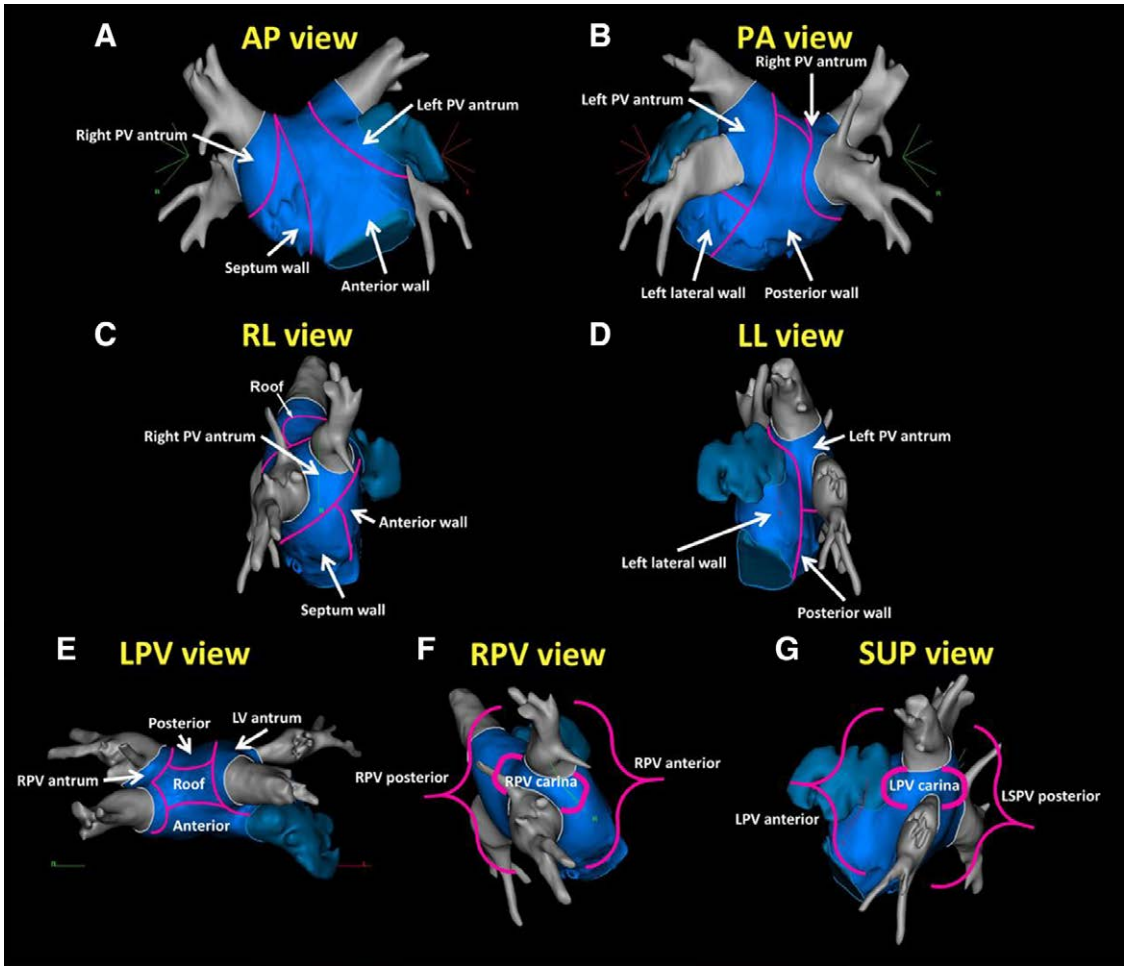

Fig. 1 The LA body was divided into five sub-segments, including the roof, posterior wall, septum, anterior wall, and left lateral wall. (A–E) Examples of the LA sub-segments. (F,G) Examples of three sub-segments of the pulmonary veins, including anterior PV antrum, carina and posterior PV antrum.

as distances between the two anatomical shells of <5 mm, 5–10 mm, and >10 mm, respectively (Fig. 2). The average quality score was calculated for each sub-segmentation of LA and PVs. We defined a quality score of 1 as regions having "perfect" matching and >1 for the remaining regions. To validate the quality score method, the inter-observer coefficient was calculated by two blinded operators.

2.6. Comparison of Contact Force between Regions with Different Quality Scores

Wide area circumferential ablation of the PVs was based on the FAM-derived geometry, and the ablation lesion was intended to target the FAM anatomic shell. During ablation, automatic ablation lesion tagging with simultaneous contact force recording was used. After ablation, the contact force of each ablation lesion was compared between perfectly matched (quality score = 1) and imperfectly matched (quality score > 1) regions.

2.7. Statistics and analysis

Data are expressed as mean ± standard deviation for normally distributed continuous variables and proportions for categorical variables. The parameters of geometries derived from different methods were compared using the Wilcoxon signed-rank test. The quality score between different sub-segmentations was analyzed using one-way ANOVA with post hoc paired comparisons. The contact force of the ablation lesions between different matched regions was analyzed using a two-tailed *t*-test. All statistical analyses were performed using SPSS version 22.0 (IBM Corporation, Armonk, NY, USA), and a p value <0.05 was considered to be statistically significant.

3. RESULTS

3.1. Phase I study

3.1.1. Patient characteristics

A total of 27 patients who underwent AF ablation (24 male, mean age 53.6 ± 8.0 years) were studied, including 22 (81.5%) with paroxysmal AF and five (18.5%) with persistent AF. With regards to the structural assessments, the mean left ventricular ejection fraction was 57.9 ± 8.2% and LA diameter was 39.7 ± 5.3 mm. Table 1 shows the baseline characteristics of the study population.

3.1.2. Comparison of LA derived from the CARTO Segmentation Module and manual segmentation of CT geometry

The longitudinal and transverse diameters of the LA calculated by manual segmentation were longer than those derived from the CARTO Segmentation Module (65.2 ± 5.6 mm vs. 62.0

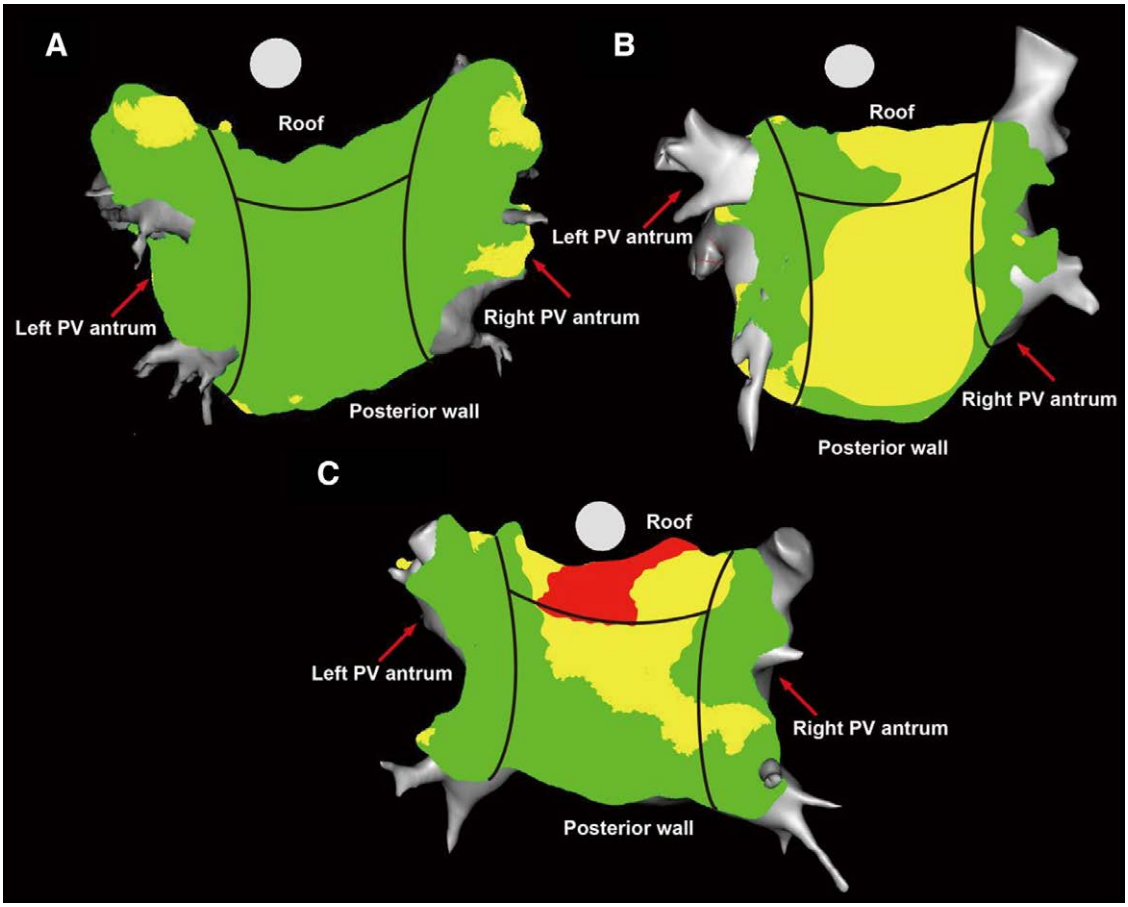

Fig. 2 Two anatomic shells derived from fast anatomical map (FAM) and CARTO segmentation-merged 3D CT geometries were analyzed and compared by Registration Match View. Quality scores of 1, 2, and 3 were defined as differences in regional contours between the two anatomical shells of <5 mm, 5–10 mm, and >10 mm, respectively. The average quality score was calculated and used for each sub-segmentation of the LA and PVs. The red, yellow, and green colors represent quality scores of 3, 2, and 1, respectively. The average quality score was calculated if two different quality scores were seen in one anatomic region. (A–C) Examples of different quality scores. A, the quality scores of the posterior wall and roof were 1; B, the quality scores of the posterior wall and roof were 2 and 1.5, respectively; C, the quality scores of the roof and posterior wall were 2.5 and 1.5, respectively.

± 14.0 mm, $p < 0.01$ and 58.1 ± 6.7 mm vs. 56.3 ± 7.0 mm, $p < 0.001$, respectively; Table 2). Furthermore, a larger cross-sectional area and longer diameters of each PV were observed in the LA calculated by manual segmentation ($p < 0.01$ for each PV, Table 2).

3.1.3. Comparison of geometries derived from the CARTO Segmentation Module and FAM

Among the five sub-segmentations of the LA body, the obtained quality score in the roof area (1.7 ± 0.6) after merging the two geometry shells was significantly higher than those in the other regions. LA anterior wall (1.1 ± 0.2) and posterior wall (1.0 ± 0.2) had the lowest quality score between the two geometries (Fig. 3A). Furthermore, among the sub-segmentation surrounding the PVs, the highest quality scores were observed surrounding the bilateral PV carinas (both 1.8 ± 0.1) (Fig. 3B).

3.2. Phase II study

3.2.1. Patient characteristics

Of the 16 patients who underwent AF ablation (10 males, mean age 58.6 ± 6.7 years), paroxysmal and persistent AF was identified in 15 (93.8%) and one (6.3%) of the patients, respectively. The left ventricular ejection fraction was 59.4 ± 4.6% and the LA diameter was 37.8 ± 4.5 mm. Table 1 shows the baseline characteristics of the study population.

3.2.2. Validation of contact force between regions with different quality scores

A total of 926 ablation lesions were acquired for validation of the contact force between regions with different quality scores, including 801 at regions with a quality score of 1 and 125 at regions with a quality score of >1. The contact force at areas with a quality score > 1 was significantly higher than that at areas with a quality score of 1 (19.9 ± 7.0 g vs 11.3 ± 4.7 g, $p < 0.05$; Fig. 4A). The higher contact force at the areas with a quality score >1 was consistent in each PV (RSPV: 20.7 ± 5.8 g vs. 12.5 ± 4.4 g; RIPV: 19.3 ± 6.8 g vs. 11.8 ± 4.8 g; LSPV: 22.5 ± 7.3 g vs. 11.2 ± 4.5 g; LIPV, 15.7 ± 6.9 g vs. 9.7 ± 4.4 g, $p < 0.05$ for each group; Fig. 4B). Regions with a quality score of >1 had more ablation lesions with a contact force >20 g comparing to those with a quality score of 1 (32.0% vs. 5.0%, $p < 0.05$; Fig. 4C).

3.2.3. Reproducibility

The inter-observer agreement in measurement of anatomic parameters and quality score yielded intra-class correlation coefficients of 0.79 and 0.98, respectively (95% confidence

Table 1

The baseline characteristics of patients in Phase I and Phase II

	Phase I (N = 27)	Phase II (N = 16)
Age, years	53.6 ± 8.0	58.6 ± 6.7
Male	24.0 (88.9%)	10.0 (62.5%)
SBP, mmHg	126.0 ± 15.6	128.9 ± 13.7
HR, bpm	79.7 ± 19.6	71.6 ± 10.5
BMI	25.7 ± 2.9	24.0 ± 2.9
eGFR, ml/min/1.73 m^2	74.3 ± 15.0	73.6 ± 14.6
AF characteristics		
Paroxysmal AF	22.0 (81.5%)	15.0 (93.8%)
Persistent AF	5.0 (18.5%)	1.0 (6.3%)
Comorbidity		
Hypertension	11.0 (40.7%)	5.0 (31.3%)
Diabetes mellitus	1.0 (3.7%)	0 (0%)
Coronary artery disease	4.0 (14.8%)	2.0 (12.5%)
Congestive heart failure	3.0 (11.1%)	1.0 (6.3%)
Stroke	2.0 (7.4%)	0 (0%)
CHA_2DS_2 VAS score	0.9 ± 0.8	1.4 ± 1.1
Echocardiography		
LA diameter, mm	39.7 ± 5.3	37.8 ± 4.5
LA volume index, mL/m^2	27.3 ± 4.0	27.0 ± 4.0
LVEF, %	57.9 ± 8.2	59.4 ± 4.6

SBP = systolic blood pressure; HR = heart rate; bpm: beats per minute; BMI = body mass index; eGFR = estimated Glomerular filtration rate; AF = atrial fibrillation; LA = left atrium; LVEF = left ventricular ejection fraction.

Table 2

The parameters of PV and LA between the 3D geometry shells created by manual CT segmentation and CARTO Segmentation Module software

	LA shell by manual CT segmentation (n = 27)	LA shell by Carto segmentation (n = 27)	*p*
RSPV diameter (mm)	19.9 ± 2.9	18.5 ± 2.9	<0.01
RSPV CSA (mm^2)	310.9 ± 6.7	268.6 ± 6.5	<0.01
LSPV diameter (mm)	21.1 ± 3.5	20.1 ± 3.5	<0.01
LSPV CSA (mm^2)	349.8 ± 9.5	317.9 ± 9.6	<0.01
RIPV diameter (mm)	18.4 ± 3.1	16.9 ± 3.0	<0.01
RIPV CSA (mm^2)	265.9 ± 7.6	225.2 ± 6.9	<0.01
LIPV diameter (mm)	17.0 ± 3.5	15.4 ± 3.0	<0.01
LIPV CSA (mm^2)	226.9 ± 9.8	187.2 ± 6.9	<0.01
LA longitudinal diameter (mm)	65.2 ± 5.6	62.0 ± 14.0	<0.01
LA transverse diameter (mm)	58.1 ± 6.7	56.3 ± 7.0	<0.01

CSA = cross-sectional area; LA = left atrium; LIPV = left inferior pulmonary vein; LSPV = left superior pulmonary vein; RIPV = right inferior pulmonary vein; RSPV = right superior pulmonary vein.

interval: 0.56 to 0.90, $p < 0.01$, and 95% CI: 0.97 to 0.99, $p < 0.01$; respectively).

4. DISCUSSION

4.1. Major findings

To the best of our knowledge, this is the first study to evaluate the impact of local LA distortion based on 3D-CARTO segmentation-derived geometries during AF ablation. There are several important findings in this study. First, there were longer LA diameters and larger cross-sectional areas of each PV created by manual segmentation than those derived from the CARTO Segmentation Module. Second, the CARTO Segmentation Module and Registration Match View provided better anatomic accuracy and less regional distortion of LA geometry. Third, the roof area and bilateral PV carinas had the highest spatial distortion. Therefore, avoiding excessive contact force when manipulating the catheter or performing ablation surrounding these regions is mandatory.

Electroanatomic mapping systems are widely used for AF ablation.[2] Merging the reconstructed LA created by a catheter with pre-procedural CT images has been shown to further improve the efficacy and safety of AF ablation, and thereby leading to better outcomes.[15,23] The new CARTO Segmentation Module provides higher spatial resolution and more accurate PV visualization, which cannot be achieved using previous images derived by merging CT with 3D electroanatomic mapping. When performing LA segmentation of CT images, separation of the LA from each PV, especially for the LA–PV junction, is important given that the influence of anatomical and positional variations of the PV structure should be avoided. The application of the CARTO Segmentation Module allows for a precise understanding of the anatomic accuracy and facilitates successful AF ablation.

In addition, the CARTO Segmentation Module is easily applicable, and image preparation is performed pre-procedurally in less than 10 minutes.[16] Manual catheter manipulation may lead to inconsistent contact forces, which can distort the virtual tissue surface and possibly increase the FAM-derived volumes.[22,24] This was demonstrated in a recent study using a robotic navigation system, which demonstrated that a stronger contact force resulted in greater distortion of the mapped volume.[7] The anatomic distortion in FAM and merged 3D CT images may further lead to misinterpretation of the local fiducial sites during mapping and ablation of complex anatomic structures.

Our results clarified the extent of anatomic distortion of 3D maps obtained via FAM compared with the CARTO Segmentation Module. Of note, the FAM-derived roof and bilateral PV carina regions were relatively far away from the corresponding locations created by the CARTO Segmentation Module. This anatomic distortion should be taken into consideration when mapping and ablation are guided by FAM. In addition, minor distortions at locations with good contact can occur due to LA wall stiffness, wall thickness, and the external force against the LA/PV wall by the surrounding tissue. Hall et al. reported that the LA roof was the thinnest region, and that this could potentially contribute to over-estimation without information on contact force, which is consistent with our findings.[25] Consequently, the distortion in FAM-derived maps and merged 3D CT images could be misrepresented. Furthermore, the current findings also emphasized the anatomic differences of each PV carina. Therefore, when creating effective lesions in the vicinity of the carina region, detailed assessment of the contact force is necessary.[26]

The accuracy of the CARTO Segmentation Module is currently not known due to factors such as differences in heart rate, rhythm, and volume status, which may result in nonuniform characteristics of the LA, particularly when CT acquisition and mapping procedures are not performed simultaneously.[27] Nevertheless, we observed a tendency for the ablation points located outside the 3D-merged CT surfaces to have a higher contact force. Consequently, the phase II study was conducted to validate the accuracy using the merged 3D images incorporating the information of contact force.

Another important factor is cardiac tamponade, which is the most common and lethal complication in patients undergoing AF ablation, with an incidence of around 1% to 3%.[28,29] Radiofrequency lesions cause fibrosis with subsequent thinning of the atrial myocardium. Therefore, a high contact force, particularly during ablation, might increase the risk of cardiac tamponade.[30] Recent studies have shown that contact force-guided

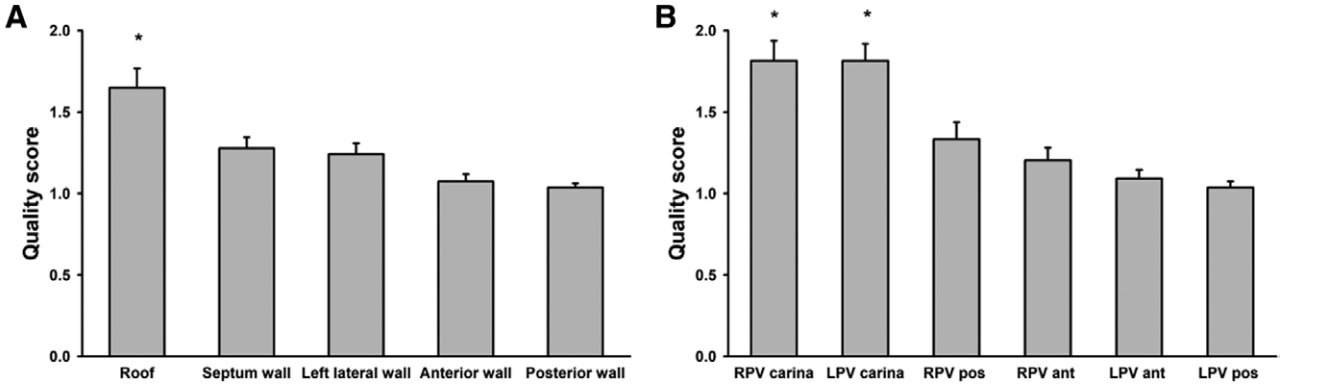

Fig. 3 (A,B) demonstrate the regional quality scores of the LA body and PV antrum between the FAM and CARTO segmentation-merged 3D CT geometries, respectively. The quality scores of the roof and PV antrum were significantly higher than those within the other regions.

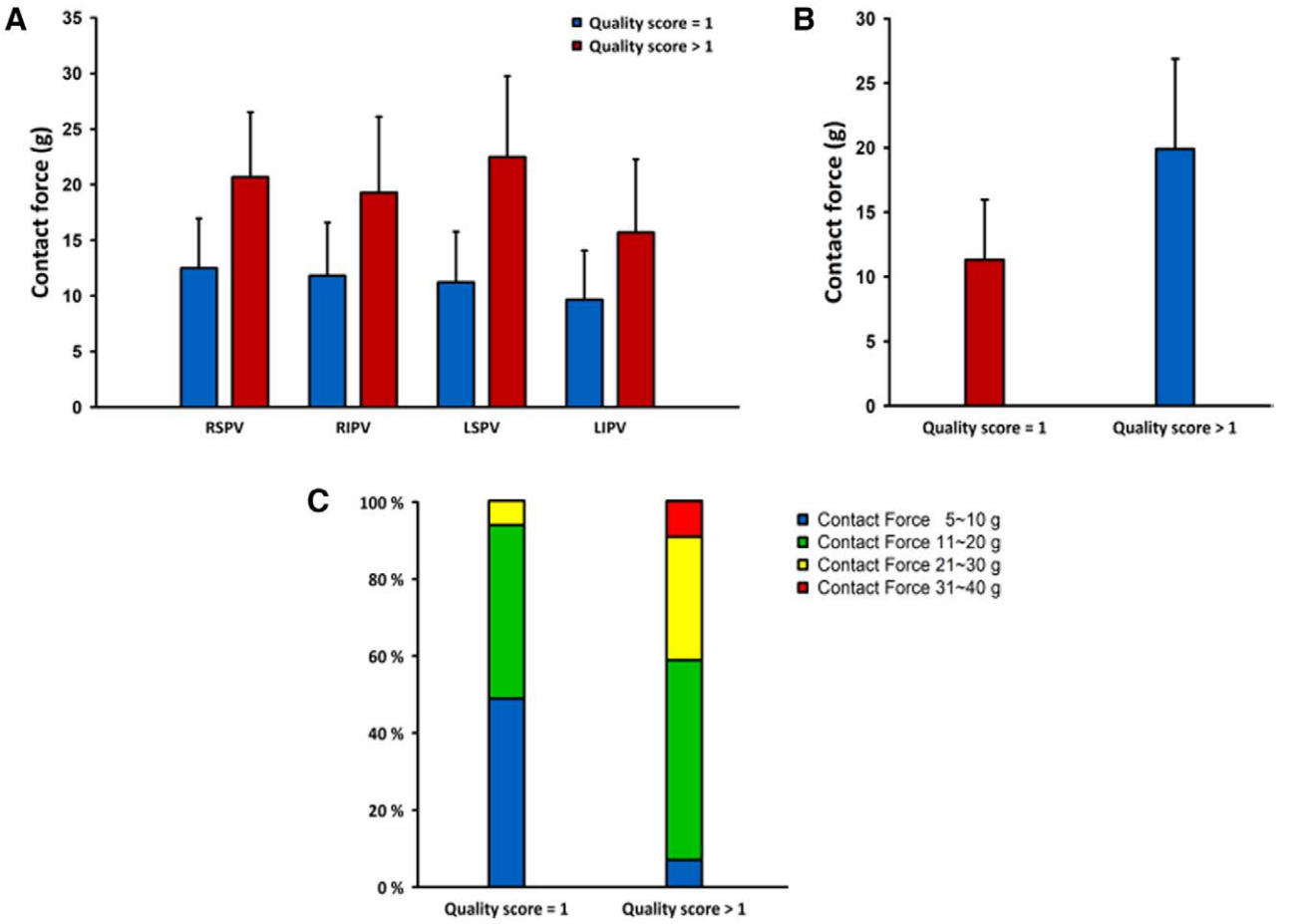

Fig. 4 (A) Comparisons of the contact force of overall ablation points between a quality score of 1 and >1. (B) Comparisons of the contact force of ablation points at each PV antrum between a quality score of 1 and >1. A higher contact force was observed for the ablation points in the FAM with a quality score >1. (C) The distribution of contact force of the ablation points with a quality score of 1 and >1.

circumferential PV isolation is safe during PV isolation procedures.[31,32] However, a contact force catheter is expensive and not affordable for every patient. Therefore, without the assistance of contact force information during AF ablation, clinicians need to avoid excessive force, particularly when manipulating catheters or ablating at the LA roof or carina region.

There are several limitations to this study. First, because CT imaging was performed prior to the ablation procedures, dynamic changes in rhythm, heart rate, contractility, or fluid state could have contributed to changes in heart size and potential registration errors. To limit these changes, we performed image registration and ablation procedures within 24 hours

after the CT scan. Second, this study was conducted at a single center, which may limit the generalizability of the results to the other centers. The results may also have been confounded by the operators' experience and skill. Third, despite the "perfectly" merged LA geometries, the absolute distances between the FAM and CARTO segmentation-merged 3D CT geometries could not be directly measured. Fourth, given the limited study population, future investigations are warranted to validate the present findings in large-scale studies

In conclusion, the CARTO Segmentation Module can help to define the exact anatomic location of the LA and PVs more accurately in AF patients, allowing for safer ablation. When the AF ablation is guided by FAM, clinicians should avoid ablation points located outside the LA surface derived from the CARTO Segmentation Module, especially for the roof and PV carina region. Our data revealed anatomic distortion of the LA shells created by different methods, and shed light on improving the safety and effectiveness of AF ablation.

ACKNOWLEDGMENTS

This work was supported by the Center for Dynamical Biomarkers and Translational Medicine, Ministry of Science and Technology (grant nos. 107-2314-B-010-061-MY2, MOST 106-2314-B-075-006-MY3, MOST 106-2314-B-010-046-MY3, and MOST 106-2314-B-075-073-MY3), Research Foundation of Cardiovascular Medicine, Szu-Yuan Research Foundation of Internal Medicine (107-02-036), Taipei Veterans General Hospital (grant numbers. V108C-032, V108C-107, V109C-113, V109D48-001-MY2-1, C17-095, V106C-158, V106C-104, V107B-014, V107C-060, and V107C-054) and Taipei Medical University – Wan Fang Hospital (109-wf-eva-18)

REFERENCES

1. Haissaguerre M, Jais P, Shah DC, Takahashi A, Hocini M, Quiniou G, et al. Spontaneous initiation of atrial fibrillation by ectopic beats originating in the pulmonary veins. *N Engl J Med* 1998;**339**:659–66.
2. Calkins H, Brugada J, Packer DL, Cappato R, Chen SA, Crijns HJ, et al. HRS/EHRA/ECAS expert consensus statement on catheter and surgical ablation of atrial fibrillation: recommendations for personnel, policy, procedures and follow-up. A report of the Heart Rhythm Society (HRS) Task Force on Catheter and Surgical Ablation of Atrial Fibrillation developed in partnership with the European Heart Rhythm Association (EHRA) and the European Cardiac Arrhythmia Society (ECAS); in collaboration with the American College of Cardiology (ACC), American Heart Association (AHA), and the Society of Thoracic Surgeons (STS). Endorsed and approved by the governing bodies of the American College of Cardiology, the American Heart Association, the European Cardiac Arrhythmia Society, the European Heart Rhythm Association, the Society of Thoracic Surgeons, and the Heart Rhythm Society. *Europace* 2007;**9**:335–79.
3. Nilsson B, Chen X, Pehrson S, Køber L, Hilden J, Svendsen JH. Recurrence of pulmonary vein conduction and atrial fibrillation after pulmonary vein isolation for atrial fibrillation: a randomized trial of the ostial versus the extraostial ablation strategy. *Am Heart J* 2006;**152**:537.e1–8.
4. Estner HL, Deisenhofer I, Luik A, Ndrepepa G, von Bary C, Zrenner B, et al. Electrical isolation of pulmonary veins in patients with atrial fibrillation: reduction of fluoroscopy exposure and procedure duration by the use of a non-fluoroscopic navigation system (NavX). *Europace* 2006;**8**:583–7.
5. Tops LF, Schalij MJ, den Uijl DW, Abraham TP, Calkins H, Bax JJ. Image integration in catheter ablation of atrial fibrillation. *Europace* 2008;**10** (**Suppl 3**):iii48–56.
6. Packer DL, Stevens CL, Curley MG, Bruce CJ, Miller FA, Khandheria BK, et al. Intracardiac phased-array imaging: methods and initial clinical experience with high resolution, under blood visualization: initial experience with intracardiac phased-array ultrasound. *J Am Coll Cardiol* 2002;**39**:509–16.
7. Okumura Y, Johnson SB, Bunch TJ, Henz BD, O'Brien CJ, Packer DL. A systematical analysis of in vivo contact forces on virtual catheter tip/tissue surface contact during cardiac mapping and intervention. *J Cardiovasc Electrophysiol* 2008;**19**:632–40.
8. Lin CY, Te ALD, Lin YJ, Chang SL, Lo LW, Hu YF, et al. High-resolution mapping of pulmonary vein potentials improved the successful pulmonary vein isolation using small electrodes and inter-electrode spacing catheter. *Int J Cardiol* 2018;**272**:90–6.
9. Hauser TH, Peters DC, Wylie JV, Manning WJ. Evaluating the left atrium by magnetic resonance imaging. *Europace* 2008;**10** (Suppl 3):iii22–7.
10. Khan F, Banchs JE, Skibba JB, Grando-Ting J, Kelleman J, Singh H, et al. Determination of left atrium volume by fast anatomical mapping and intracardiac echocardiography. The contribution of respiratory gating. *J Interv Card Electrophysiol* 2015;**42**:129–34.
11. Higuchi K, Cates J, Gardner G, Morris A, Burgon NS, Akoum N, et al. The spatial distribution of late gadolinium enhancement of left atrial magnetic resonance imaging in patients with atrial fibrillation. *JACC Clin Electrophysiol* 2018;**4**:49–58.
12. Anjo N, Nakahara S, Okumura Y, Hori Y, Nagashima K, Komatsu T, et al. Impact of catheter tip-tissue contact on three-dimensional left atrial geometries: relationship between the external structures and anatomic distortion of 3D fast anatomical mapping and high contact force guided images. *Int J Cardiol* 2016;**222**:202–8.
13. Osmanagic A, Möller S, Osmanagic A, Sheta HM, Vinther KH, Egstrup K. Left atrial sphericity index predicts early recurrence of atrial fibrillation after direct-current cardioversion: an echocardiographic study. *Clin Cardiol* 2016;**39**:406–12.
14. Hauser TH, Essebag V, Baldessin F, McClennen S, Yeon SB, Manning WJ, et al. Prognostic value of pulmonary vein size in prediction of atrial fibrillation recurrence after pulmonary vein isolation: a cardiovascular magnetic resonance study. *J Cardiovasc Magn Reson* 2015;**17**:49.
15. Tops LF, Bax JJ, Zeppenfeld K, Jongbloed MR, Lamb HJ, van der Wall EE, et al. Fusion of multislice computed tomography imaging with three-dimensional electroanatomic mapping to guide radiofrequency catheter ablation procedures. *Heart Rhythm* 2005;**2**:1076–81.
16. Tovia-Brodie O, Belhassen B, Glick A, Shmilovich H, Aviram G, Rosso R, et al. Use of New Imaging CARTO® Segmentation Module Software to Facilitate Ablation of Ventricular Arrhythmias. *J Cardiovasc Electrophysiol* 2017;**28**:240–8.
17. Zhou M, Liao Y, Tu X. The role of transcription factors in atrial fibrillation. *J Thorac Dis* 2015;**7**:152–8.
18. Lahvic JL, Ji Y, Marin P, Zuflacht JP, Springel MW, Wosen JE, et al. Small heat shock proteins are necessary for heart migration and laterality determination in zebrafish. *Dev Biol* 2013;**384**:166–80.
19. Scaglione M, Biasco L, Caponi D, Anselmino M, Negro A, Di Donna P, et al. Visualization of multiple catheters with electroanatomical mapping reduces X-ray exposure during atrial fibrillation ablation. *Europace* 2011;**13**:955–62.
20. Dong J, Dickfeld T, Dalal D, Cheema A, Vasamreddy CR, Henrikson CA, et al. Initial experience in the use of integrated electroanatomic mapping with three-dimensional MR/CT images to guide catheter ablation of atrial fibrillation. *J Cardiovasc Electrophysiol* 2006;**17**:459–66.
21. Dong J, Calkins H, Solomon SB, Lai S, Dalal D, Lardo AC, et al. Integrated electroanatomic mapping with three-dimensional computed tomographic images for real-time guided ablations. *Circulation* 2006;**113**:186–94.
22. Okumura Y, Henz BD, Johnson SB, Bunch TJ, O'Brien CJ, Hodge DO, et al. Three-dimensional ultrasound for image-guided mapping and intervention: methods, quantitative validation, and clinical feasibility of a novel multimodality image mapping system. *Circ Arrhythm Electrophysiol* 2008;**1**:110–9.
23. Kistler PM, Earley MJ, Harris S, Abrams D, Ellis S, Sporton SC, et al. Validation of three-dimensional cardiac image integration: use of integrated CT image into electroanatomic mapping system to perform catheter ablation of atrial fibrillation. *J Cardiovasc Electrophysiol* 2006;**17**:341–8.
24. Ryu K, D'Avila A, Heist EK, Rosenberg SP, Chou J, Yang M, et al. Simultaneous electrical and mechanical mapping using 3D cardiac mapping system: novel approach for optimal cardiac resynchronization therapy. *J Cardiovasc Electrophysiol* 2010;**21**:219–22.
25. Hall B, Jeevanantham V, Simon R, Filippone J, Vorobiof G, Daubert J. Variation in left atrial transmural wall thickness at sites commonly targeted for ablation of atrial fibrillation. *J Interv Card Electrophysiol* 2006;**17**:127–32.

26. Okumura Y, Watanabe I, Kofune M, Nagashima K, Sonoda K, Mano H, et al. Effect of catheter tip-tissue surface contact on three-dimensional left atrial and pulmonary vein geometries: potential anatomic distortion of 3D ultrasound, fast anatomical mapping, and merged 3D CT-derived images. *J Cardiovasc Electrophysiol* 2013;**24**:259–66.
27. Ector J, De Buck S, Adams J, Dymarkowski S, Bogaert J, Maes F, et al. Cardiac three-dimensional magnetic resonance imaging and fluoroscopy merging: a new approach for electroanatomic mapping to assist catheter ablation. *Circulation* 2005;**112**:3769–76.
28. Cappato R, Calkins H, Chen SA, Davies W, Iesaka Y, Kalman J, et al. Worldwide survey on the methods, efficacy, and safety of catheter ablation for human atrial fibrillation. *Circulation* 2005;**111**:1100–5.
29. Cappato R, Calkins H, Chen SA, Davies W, Iesaka Y, Kalman J, et al. Updated worldwide survey on the methods, efficacy, and safety of catheter ablation for human atrial fibrillation. *Circ Arrhythm Electrophysiol* 2010;**3**:32–8.
30. Baman TS, Jongnarangsin K, Chugh A, Suwanagool A, Guiot A, Madenci A, et al. Prevalence and predictors of complications of radiofrequency catheter ablation for atrial fibrillation. *J Cardiovasc Electrophysiol* 2011;**22**:626–31.
31. Kimura M, Sasaki S, Owada S, Horiuchi D, Sasaki K, Itoh T, et al. Comparison of lesion formation between contact force-guided and non-guided circumferential pulmonary vein isolation: a prospective, randomized study. *Heart Rhythm* 2014;**11**:984–91.
32. Itoh T, Kimura M, Tomita H, Sasaki S, Owada S, Horiuchi D, et al. Reduced residual conduction gaps and favourable outcome in contact force-guided circumferential pulmonary vein isolation. *Europace* 2016;**18**:531–7.